# Source Localization Using Virtual Antenna Arrays

Yaqoob, Muhammad Atif; Mannesson, Anders; Butt, Naveed R.; Tufvesson, Fredrik

*Published in:*
2015 International Conference on Localization and GNSS (ICL-GNSS)

*DOI:*
10.1109/ICL-GNSS.2015.7217142

2015

# Source Localization Using Virtual Antenna Arrays

Muhammad Atif Yaqoob*, Anders Mannesson†, Naveed R. Butt‡, Fredrik Tufvesson*
*Dept. of Electrical and Information Technology, Lund University, Lund, Sweden
†Dept. of Automatic Control, Lund University, Lund, Sweden
‡Ericsson AB, Lund, Sweden
Email: Atif.Yaqoob@eit.lth.se

***Abstract*—Using antenna arrays for direction of arrival (DoA) estimation and source localization is a well-researched topic. In this paper, we analyze virtual antenna arrays for DoA estimation where the antenna array geometry is acquired using data from a low-cost inertial measurement unit (IMU). Performance evaluation of an unaided inertial navigation system with respect to individual IMU sensor noise parameters is provided using a state space based extended Kalman filter. Secondly, using Monte Carlo simulations, DoA estimation performance of random 3-D antenna arrays is evaluated by computing Cramér-Rao lower bound values for a single plane wave source located in the far field of the array. Results in the paper suggest that larger antenna arrays can provide significant gain in DoA estimation accuracy, but, noise in the rate gyroscope measurements proves to be a limiting factor when making virtual antenna arrays for DoA estimation and source localization using single antenna devices.**

***Index Terms*—Virtual Antenna Array, Localization, Inertial Measurement Unit, Unaided Inertial Navigation System, Direction of Arrival, Angle of Arrival**

## I. Introduction

Direction of arrival (DoA) information at an antenna array of a mobile station is very useful for positioning purposes. DoA information can be directly used for triangulation to find the position of the mobile station in a given frame of reference. In [1], a random 3-D antenna array is used for DoA estimation, where, a virtual antenna array is formed by moving a single receive antenna in 3-D and estimating the antenna position coordinates from inertial measurement unit (IMU) measurements. Furthermore, in [2], [3], the effect of IMU sensor noise on the allowable time-duration of the virtual antenna trajectory, and consequently, on DoA estimation is provided. It has been shown that the length of the virtual antenna arrays is limited by the growing standard deviation of the antenna position errors. For an unaided inertial navigation system the standard deviation of the position estimation error grows over time if there is not any periodic correction made to the estimated position. However, the estimated position with small to moderately large position errors can be obtained for small integration times for which the uncertainty of the estimated position remains within a specified limit [2], [4].

Several authors have made contributions in the literature for DoA estimation with antenna arrays having antenna position perturbations. In [5], the authors have provided a discussion on the optimality of a delay-and-sum beamformer for antenna arrays with random antenna position perturbations. If the antenna position errors are assumed to be random at different antenna positions, their influence can be considered as if the signal to noise ratio (SNR) of the received radio signal is decreased. It has been shown that, for small to moderately large errors, conventional delay-and-sum beamforming would be optimal to estimate DoA of a single source located in the far field of the array. In [6], [7], [8], the authors have considered a scenario where more than one source is present transmitting the radio signal and the array is perturbed with small to moderately large antenna position errors. In those references, the authors have suggested that antenna array calibration and DoA estimation can be performed simultaneously with some underlying assumptions to fulfill the identifiability criterion for the joint estimation of antenna position errors and DoA of the incoming radio signal.

Our first main contribution in this paper is to investigate the effect of each individual IMU noise source on the performance of an unaided inertial navigation system. For this purpose, using the extended Kalman filter (EKF) that has been formulated in [2], we provide a detailed study of the effect of individual IMU noise sources on the unaided navigation system performance. Acceleration and rate gyroscope measurements from the IMU are used allowing six degrees of freedom inertial navigation system. In [9], the authors have analyzed mean drift in the static IMU position using Monte Carlo simulations where the IMU was considered static and stochastic errors in the IMU data are used as measurements from the IMU. Another approach in the literature is to derive complex analytical expressions to determine the effect of IMU noise sources on the navigation system performance [4]. We provide a direct and simple approach to analyze the results of position estimation error standard deviation vs. time of an unaided inertial navigation system w.r.t the different IMU sensor noise parameters using an EKF.

It is also of interest to study how the DoA estimation or source localization problem is affected by the shape of a virtual antenna array. In this regard, our second contribution is to provide a detailed Cramér-Rao lower bound (CRLB)-based study of DoA estimation from random 3-D antenna arrays assuming perfect knowledge of the antenna elements. We provide mean standard deviation of the DoA estimation error for random 3-D antenna arrays using Monte Carlo simulations. Different SNR values and different array lengths in terms of allowed time-duration for making virtual antenna arrays are considered for the simulations.

Our idea is to to make virtual antenna array where the antenna location is tracked using IMU measurements of acceleration and angular speed for short integration times; and then doing DoA estimation for positioning and source localization purposes. The paper discusses fundamental limitations of this technique and brief results about the achievable accuracy of DoA estimation using such antenna arrays are provided. The results from the first part of the study helps us to identify the allowed time-duration for making the virtual antenna array using the IMU measurements. While, the second part discusses about the mean DoA estimation performance that can be achieved using random 3-D antenna arrays if a single source is present in the far field.

The paper is organized as follows. Section II demonstrates how the IMU data is simulated for random trajectories in 3-D. The effect of IMU measurement noise on the unaided inertial navigation system performance is determined in Section III. A brief description on the use of CRLB followed by Monte Carlo simulation results for DoA estimation are given in Section IV. Finally, a summary of results, and conclusion are given in Section V.

## II. IMU Data Generation

Using the Singer motion model, which can be used to model maneuvering of a moving object having time correlated acceleration, a random trajectory can be made in 3-D as described in [2], [10], [11]. With the Singer model, acceleration and rotation rate data samples are generated with a first-order Gauss-Markov process. The discrete-time equivalent for the acceleration data samples is given as [10], [11]

$$\mathbf{a}_{k+1}=a_d\mathbf{a}_k + b_d\nu_{\mathbf{a}_k}, \tag{1}$$

where $\mathbf{a}_k \in \mathbb{R}^3$ is the acceleration at time index $k$, $a_d=e^{-\frac{T_s}{\tau_a}}$, $b_d=\int_0^{T_s} e^{-\frac{t}{\tau_a}}dt$, $\nu_{\mathbf{a}_k}$ is white Gaussian noise at time index $k$, $T_s$ is the sample time, and $\tau_a$ is the maneuver time constant. The variance of the moving object's acceleration $\sigma_{acc}^2$ can be defined as [10]

$$\sigma_{acc}^2 = \frac{a_{\max}^2}{3}(1+4P_{\max}-P_0), \tag{2}$$

where $a_{\max}$ is the maximum acceleration during object's maneuver; $P_{\max}$ and $P_0$ model the probability of having maximum acceleration and zero acceleration during the maneuver. $\sigma_{\nu_\mathbf{a}}^2$, the variance of the white Gaussian noise process that drives the Gauss-Markov process in (1) is computed as

$$\sigma_{\nu_\mathbf{a}}^2 = \frac{1-a_d^2}{b_d^2}\sigma_{acc}^2. \tag{3}$$

Similarly, rotation rate data samples are generated as well using the Singer model.

### A. Random 3-D Antenna Array Coordinates

Using the Singer model, acceleration and rotation rate data is generated for each of the three coordinate axis. For a typical movement by holding an IMU in hand (e.g. a smart phone equipped with an IMU and a single antenna receiver), values of the different parameters in the Singer model are set as $\tau_a$=2.5 s, $a_{\max}$=1 m/s$^2$, $P_0$=0.99, and $P_{\max}$=0.01. For rotation rate data, the maximum angular speed is set as $w_{max}$=600 deg/s while the remaining parameters are the same as are used for the acceleration data. Similar parameter settings for each of the three coordinate axis are used for the acceleration as well as for the angular speed. A sample realization of the simulated acceleration during 10 seconds is shown in Fig. 1 for each of the three coordinate axes. Simple double integration of the acceleration along each of these three coordinate axes provides the position displacement in each axis as shown in Fig. 2. A 3-D plot of the same position displacement data is shown in Fig. 3, where the origin is defined at the center of gravity of the array.

## III. IMU Sensor Noise and Inertial Navigation System Simulation

For a low cost MEMS based IMU, white Gaussian noise and bias instability in the IMU measurements are the main sources of errors in the position estimates in an unaided inertial navigation system for short integration times [2]. These stochastic errors are typically quantified using Allan variance analysis [12], [13]. Using static IMU data as shown in [2], their numerical values are calculated and are given in Table I. The IMU used in the measurements is a Phidget-1044 which is a

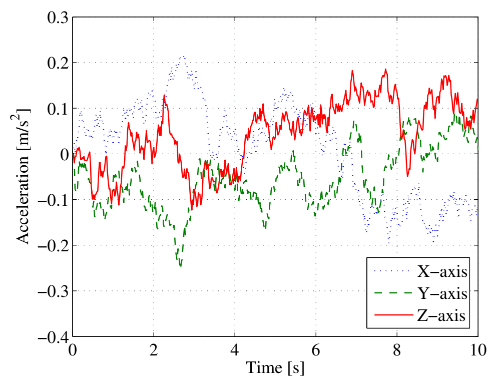


Fig. 1. Example plot of acceleration data in Cartesian coordinates using the Singer model.

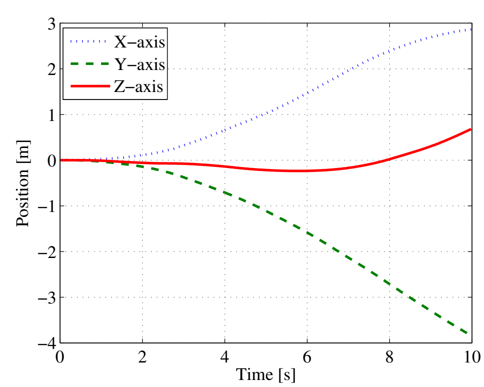


Fig. 2. Position displacement calculated by double integration of the acceleration data shown in Fig. 1.

low cost MEMS based IMU and it provides 3-axis acceleration and rotation rate measurements [14].

TABLE I
NOISE PARAMETERS FOR ACCELEROMETER AND GYROSCOPE [2]

| | VRW / ARW | Bias Instability |
|---|---|---|
| Accelerometer | $5.86\times10^{-4}$ m/s/$\sqrt{\text{s}}$ | $2.85\times10^{-4}$ m/s$^2$(at 115 s) |
| Gyroscope | $1.63\times10^{-2}$ deg /$\sqrt{\text{s}}$ | $7.5\times10^{-3}$ deg /s(at 115 s) |

The sensor noise parameters in Table I are used as nominal noise parameters to simulate noise in the acceleration and rotation rate data samples in the following subsections. Using the state space model in the EKF, antenna position coordinates are estimated along-with other parameters in the state vector. After each iteration of the EKF, the estimation error covariance matrix is also obtained for the parameters in the state vector. Position estimation error standard deviation results from the EKF are then used to investigate the effects of stochastic errors in the accelerometer and rate gyroscope measurements, as given in the following sections III-A, III-B and III-C.

## A. Accelerometer Noise

In order to investigate the effect of accelerometer noise on the position estimation error, it is assumed that the device's initial orientation is known and that there is no noise in the gyroscope measurements.

*1) Velocity Random Walk (VRW):* By using the nominal value of the VRW noise parameter given in Table I and setting the bias instability noise in the accelerometer measurements to zero, the state vector is estimated from the EKF along-with the estimation error covariance matrix. Fig. 4 shows the standard deviation of the position estimation error vs. time for each of the three coordinate axes. It can be noted from the plots that all of the three coordinate axes overlap each other. This suggests that if the accelerometer white Gaussian noise is the only noise source in the IMU measurements, then similar position estimation error will be observed for each of the three coordinate axes. Furthermore, by changing the VRW noise parameter to twice and half of the nominal value, the position estimation error standard deviation results from the EKF are obtained as shown in Fig. 4. These results indicate that the standard deviation of the position estimation error is directly proportional to the VRW noise parameter.

*2) Acceleration Bias Drift:* By using the nominal value of the bias instability noise parameter for the accelerometer measurements given in Table I and setting the VRW noise parameter to zero, the state vector is estimated from the EKF along-with the estimation error covariance matrix. Fig. 5 shows the standard deviation of the position estimation error vs. time for each of the three coordinate axes. The plots show that the position estimation error for the three coordinate axes is different in each axis. Due to the fact that the bias drift is a time correlated process and it is independent in each axis, different position estimation error standard deviation results are observed for each axis. Further, by varying the standard deviation of the white Gaussian noise that drives the accelerometer bias drift process, results for the standard deviation of the position estimation error are also obtained from the EKF as shown in Fig. 5. These results illustrate that the standard deviation of the position estimation error is directly proportional to the bias instability noise parameters.

*3) VRW and Acceleration Bias Drift:* By using the nominal values of the VRW and bias instability noise parameters for the accelerometer measurements given in Table I, the state vector is estimated from the EKF along-with the estimation error covariance matrix. Fig. 6 shows the standard deviation of the position estimation error vs. time for each of the three coordinate axes. From the plot it can be noted that the VRW is the dominant error source as compared to the acceleration bias drift in unaided inertial navigation system for short integration times of about 4-6 s.

## B. Gyroscope Noise

In order to investigate the effect of gyroscope noise on the position estimation error, it is assumed that the device's

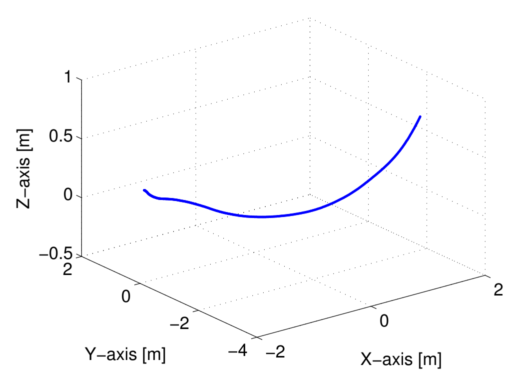


Fig. 3. Trajectory from position estimates shown in Fig. 2 plotted in 3-D. Origin is defined at the center of gravity of the array.

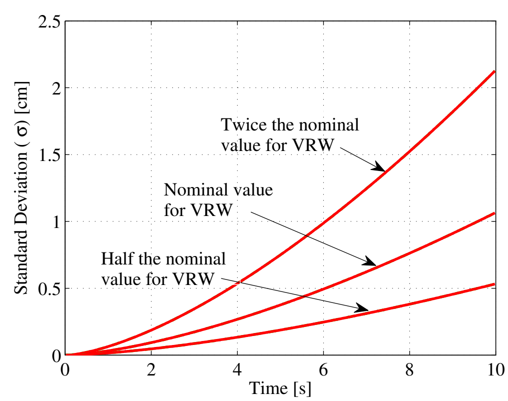


Fig. 4. Plot of the standard deviation of the position estimation error for the three coordinate axes vs. time with VRW noise only. All the three coordinate axes curves overlap each other with VRW noise only in the IMU measurements. The VRW noise parameter is also changed from the nominal value given in Table I to study its effect on the navigation system performance.

initial orientation is known and that there is no noise in the accelerometer measurements.

*1) Angle Random Walk:* By using the nominal value of the ARW noise parameter given in Table I and setting the bias instability noise in the gyroscope measurements to zero, the state vector is estimated from the EKF along-with the estimation error covariance matrix. Fig. 7 shows the standard deviation of the position estimation error vs. time for each of the three coordinate axes. From the plot, it can be observed that the estimation error standard deviations in the horizontal axes are larger as compared to the vertical axis. Any tilt error $\zeta$ in the orientation estimate of the IMU projects the gravity acceleration incorrectly onto the horizontal axes and vertical axis. The component of gravity acceleration onto the horizontal axes is projected as $g\sin(\zeta)$, while the component that is projected onto the vertical axis is $g(1-\cos(\zeta))$. Using small angle approximation, $\sin(\zeta) \approx \zeta$ and $\cos(\zeta) \approx 1$, which means that the residual acceleration due to gravity along the horizontal axes is larger as compared to the vertical axis. This leads to larger position estimation errors along the horizontal axes as compared to the vertical axis. Similar results can be found in [9]. Furthermore, by changing the ARW noise parameter to twice and half of the nominal value, the position estimation error standard deviation results from the EKF are obtained as shown in Fig. 7. These results indicate that the standard deviation of the position estimation error is directly proportional to the ARW noise parameter.

*2) Rotation Rate Bias Drift:* By using the nominal value of the bias instability noise parameter for the gyroscope measurements given in Table I and setting the ARW noise parameter to zero, the state vector is estimated from the EKF along-with the estimation error covariance matrix. Fig. 8 shows the standard deviation of the position estimation error vs. time for each of the three coordinate axes. Due to the bias drift, tilt errors result in the orientation estimate and consequently residual accelerations due to gravity in each of the coordinate axes. Fig. 8 shows that the position estimation error standard deviations in the horizontal axes are also larger as compared to the vertical axis due to the bias drift in the gyroscope measurements. The explanation is similar as given in Section III-B1. Further, by varying the standard deviation of the white Gaussian noise that drives the gyroscope bias drift process, results for the standard deviation of the position estimation error are also obtained from the EKF as shown in Fig. 8. These results indicate that the standard deviation of the position estimation error is directly proportional to the bias instability noise parameters.

*3) ARW and Rotation Rate Bias Drift:* By using the nominal values of the ARW and bias instability noise parameters for the gyroscope measurements given in Table I, the state vector is estimated from the EKF along-with the estimation error covariance matrix. Fig. 9 shows the standard deviation of the position estimation error vs. time for each of the three coordinate axes. From the plot it can be noted that the ARW is the dominant error source as compared to the gyroscope bias

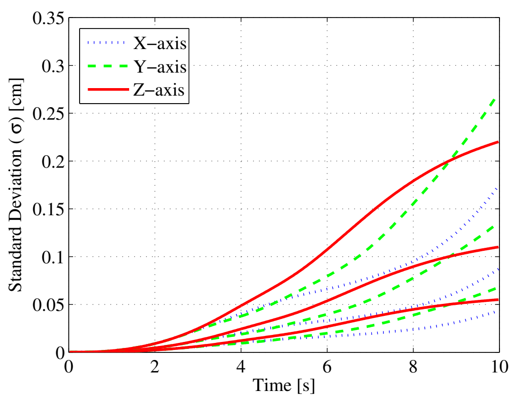


Fig. 5. Plot of the standard deviation of the position estimation error for the three coordinate axes vs. time with bias instability noise only. Bias instability noise parameter is also changed from the nominal value given in Table I to study its effect onto the navigation system performance.

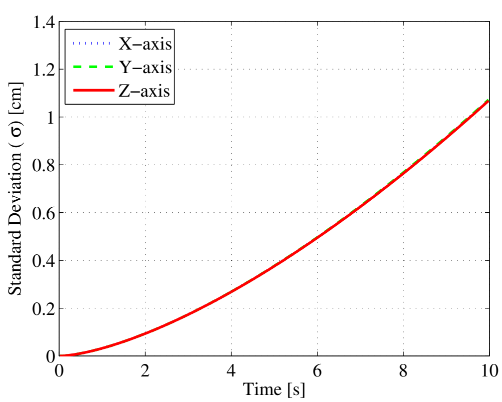


Fig. 6. VRW and bias instability noise in the accelerometer measurements is considered using nominal values as given in Table I. Plot of the standard deviation of the position estimation error for the three coordinate axes vs. time with accelerometer noise only.

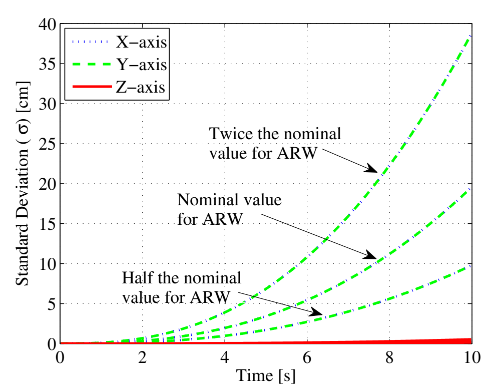


Fig. 7. Plot of the standard deviation of the position estimation error for the three coordinate axes vs. time with ARW noise only. The x- and y-axis plots overlap each other while the z-axis has smaller standard deviation as compared to the horizontal axes. The ARW noise parameter is also changed from the nominal value given in Table I to study its effect on the navigation system performance.

drift in unaided inertial navigation system for short integration times of about 4-6 s.

### C. Both Accelerometer and Gyroscope Noises

By using the nominal values of the accelerometer and the gyroscope noise parameters given in Table I, the state vector is estimated from the EKF along-with the estimation error covariance matrix. Fig. 10 shows the standard deviation of the position estimation error vs. time for each of the three coordinate axes. The plot shows how the standard deviation of the position estimation error grows over time for an unaided inertial navigation system. It can be noted that the noise in the gyroscope measurements or more specifically the white Gaussian noise or ARW in the rate gyroscope measurements is the dominant error source in unaided inertial navigation systems for short integration times of about 4-6 s.

## IV. DoA Estimation using Monte Carlo Simulations

Using a minimum variance unbiased estimator, the direction of arrival estimate of an incoming radio signal received at an antenna array will be an optimal estimate in the maximum likelihood sense. The CRLB provides us such lower bound on the minimum variance that can be achieved with a maximum likelihood estimator. We will use the same formulation as in [2] to calculate the CRLB for a random antenna array of $N$ isotropic antenna elements whose locations are known and are placed randomly in 3-D. In the calculations, the radio signal carrier frequency is set to 2.4 GHz.

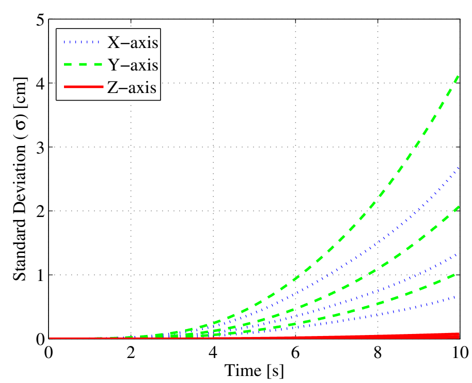


Fig. 8. Plot of the standard deviation of the position estimation error for the three coordinate axes vs. time with bias instability noise. The bias instability noise parameter is also changed from the nominal value given in Table I to study its effect onto the navigation system performance.

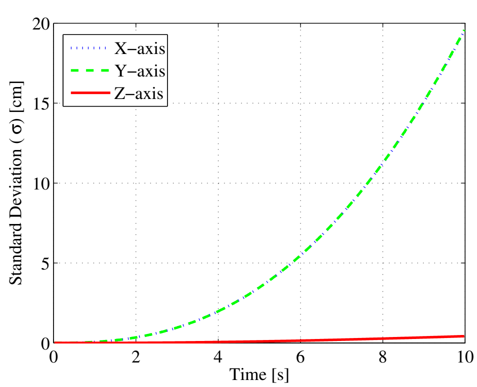


Fig. 9. Plot of the standard deviation of the position estimation error for the three coordinate axes vs. time with gyroscope noise only when ARW and bias instability noise in the gyroscope measurements is considered.

Monte Carlo simulation results are used to analyze the performance of random antenna arrays in 3-D for DoA estimation. Firstly, this section provides a brief illustration of DoA estimation performance using random 3-D antenna arrays. Using 10 Monte Carlo simulations, random 3-D antenna array coordinates are obtained for 10 different antenna arrays. As described in Section II-A, acceleration data is generated for 4 seconds using the Singer model and direct double integration of the acceleration data is performed to obtain the true antenna locations of the virtual array. Using the generated antenna arrays, CRLB results for DoA estimation are then computed for different source locations and the results are shown in Fig. 11. In Fig. 11, different colors are used for 10 different antenna arrays. Without any loss of generality, the source Elevation angle is fixed at $\theta = 30^\circ$ while the Azimuth angle $\phi$ is varied from $10^\circ$ - $360^\circ$ with a step of $10^\circ$. The plots in Fig. 11 show lower bound on the achievable DoA estimation accuracy for a single plane wave source located in the far field of the array at different source locations, for 10 different antenna arrays. It can be noted that the effect of antenna array aperture w.r.t the source location plays a significant role in DoA estimation accuracy. It is also worth mentioning that the model used to make random array shapes puts no constraint on the volume spanned by the antenna array coordinates. Furthermore, using 500 Monte Carlo simulations, the mean standard deviation $\sigma_{avg}$ of the DoA estimation error is calculated for random 3-D antenna arrays as

$$\sigma_{avg} = \frac{1}{500}\sum_{i=1}^{500}\sigma_i, \tag{4}$$

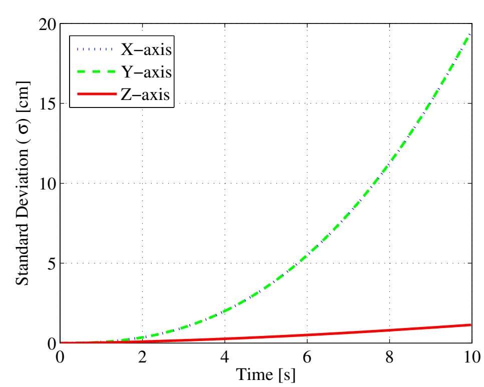


Fig. 10. Plot of the standard deviation of the position estimation error for the three coordinate axes vs. time. Accelerometer and gyroscope noise in the IMU measurements is considered using nominal values given in able I. The plot shows the effect of all the noise sources in the accelerometer and rate gyroscope measurements.

where $\sigma_i$ describes the mean DoA estimation performance for the $i^{\text{th}}$ antenna array in the Monte Carlo simulations. $\sigma_i$ is found by computing the CRLB values for different source locations, where the Elevation angle is fixed at $30^\circ$ and the Azimuth angle is varied from $10^\circ$ - $360^\circ$ with a step of $10^\circ$. By averaging the CRLB values corresponding to different source locations, the mean CRLB value $\sigma_i$ is then determined. Table II shows the results of $\sigma_{avg}$ for different array lengths in terms of time-duration for making virtual antenna arrays and for different SNR values.

TABLE II
MEAN STANDARD DEVIATION $\sigma_{avg}$ OF THE DOA ESTIMATION ERROR USING RANDOM 3-D ANTENNA ARRAYS.

| SNR [dB] | 0 | | 10 | |
|---|---|---|---|---|
| Array Length [s] | 4 | 6 | 4 | 6 |
| $\sigma_{avg}$ [deg] | 8.8 | 3.1 | 2.8 | 1.0 |

The results in Table II illustrate the mean or the average performance of random 3-D antenna arrays for DoA estimation. One antenna array could have better DoA estimation accuracy in certain source location directions and worse DoA estimation accuracy in some other source directions. An array shape in 3-D might be devised for optimum DoA estimation for all azimuth-elevation source directions. The results in Table II further show that the array performance for DoA estimation improves significantly with increased array size as compared to the increase in SNR. Similarly, for other values of the Elevation angle, the mean standard deviation of the DoA estimation error results can be obtained using the Monte Carlo simulations.

## V. SUMMARY AND CONCLUSION

In this paper, we have shown the application of a state space based extended Kalman filter to study the effect of individual IMU sensor noise parameters on the performance of an unaided inertial navigation system. We have observed that, for a typical low cost MEMS based IMU, noise in the rate gyroscope measurements is the dominant error source for the position estimation error for short integration times of about 4-6 s. Whereas, the accelerometer noise is observed to be less significant as compared to the rate gyroscope noise. We have also used Monte Carlo simulations to analyze the mean standard deviation of the DoA estimation error for random 3-D antenna arrays. Simulation results show that the array performance for DoA estimation improves significantly with increased array size as compared to the increase in signal to noise ratio. The results in the paper suggest that larger antenna arrays can provide significant gain in DoA estimation accuracy, but, noise in the rate gyroscope measurements proves to be the limiting factor when making virtual antenna arrays for DoA estimation or source localization using single antenna devices.

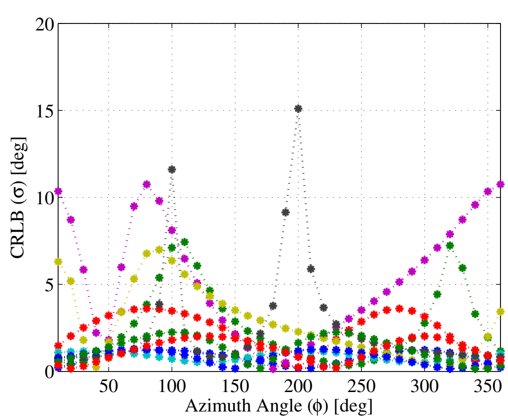


Fig. 11. Plot of CRLB values w.r.t the source location angles for 10 different 3-D antenna arrays. Different colors correspond to different antenna arrays.


## ACKNOWLEDGMENT

This work is supported by the Excellence Center at Linköping-Lund in Information Technology (www.elliit.liu.se) and by the Lund Center for Control of Complex Engineering Systems (www.lccc.lth.se) as well as the Swedish Research Council. The support is gratefully acknowledged.


## REFERENCES


[1] M. Yaqoob, F. Tufvesson, A. Mannesson, and B. Bernhardsson, "Direction of arrival estimation with arbitrary virtual antenna arrays using low cost inertial measurement units," in *2013 IEEE International Conference on Communications Workshops (ICC)*, June 2013, pp. 79–83.

[2] M. Yaqoob, A. Mannesson, B. Bernhardsson, N. Butt, and F. Tufvesson, "On the performance of random antenna arrays for direction of arrival estimation," in *2014 IEEE International Conference on Communications Workshops (ICC)*, June 2014, pp. 193–199.

[3] A. Mannesson, B. Bernhardsson, M. Yaqoob, and F. Tufvesson, "Optimal virtual array length under position imperfections," in *2014 IEEE 8th Sensor Array and Multichannel Signal Processing Workshop (SAM)*, June 2014, pp. 5–8.

[4] D. Titterton and J. L. Weston, *Strapdown inertial navigation technology*, 2nd ed. IET, 2004.

[5] P. M. Schultheiss and J. P. Ianniello, "Optimum range and bearing estimation with randomly perturbed arrays," *Acoustical Society of America Journal*, vol. 68, pp. 167–173, Jul. 1980.

[6] Y. Rockah and P. Schultheiss, "Array shape calibration using sources in unknown locations–part I: Far-field sources," *IEEE Trans. Acoust., Speech, Signal Process.*, vol. 35, no. 3, pp. 286–299, Mar 1987.

[7] B. P. Flanagan and K. L. Bell, "Array self-calibration with large sensor position errors," *Signal Processing*, vol. 81, no. 10, pp. 2201–2214, 2001.

[8] P.-J. Chung and S. Wan, "Array self-calibration using SAGE algorithm," in *2008 IEEE 5th Sensor Array and Multichannel Signal Processing Workshop (SAM)*, July 2008, pp. 165–169.

[9] O. J. Woodman, "An introduction to inertial navigation," *University of Cambridge, Computer Laboratory, Tech. Rep. UCAMCL-TR-696*, 2007.

[10] X. Li and V. Jilkov, "Survey of maneuvering target tracking. Part I: Dynamic models," *IEEE Trans. Aerosp. Electron. Syst.*, vol. 39, no. 4, pp. 1333–1364, 2003.

[11] R. Singer, "Estimating optimal tracking filter performance for manned maneuvering targets," *IEEE Trans. Aerosp. Electron. Syst.*, vol. AES-6, no. 4, pp. 473–483, July 1970.

[12] D. Allan, "Statistics of atomic frequency standards," *Proc. IEEE*, vol. 54, no. 2, pp. 221–230, 1966.

[13] N. El-Sheimy, H. Hou, and X. Niu, "Analysis and modeling of inertial sensors using Allan variance," *IEEE Trans. Instrum. Meas.*, vol. 57, no. 1, pp. 140–149, 2008.

[14] "Phidgets inc. - 1044_0 - phidgetspatial precision 3/3/3 high resolution," Retrieved March 16, 2015. [Online]. Available: http://www.phidgets.com/products.php?product_id=1044